KARL-FRANZENS-UNIVERSITÄT GRAZ
UNIVERSITY OF GRAZ

Magnetic helicity as indicator for solar eruptivity

J. K. Thalmann[1]

L. Linan[2], K. Moraitis[2], X. Sun[3], E. Pariat[2], G. Valori[4], M. Gupta[1], K. Dalmasse[5]

[1] University of Graz, Institute of Physics/IGAM, Austria
[2] LESIA, Observatoire de Paris, Universite PSL, CNRS, Sorbonne Universite, Universite de Paris, France
[3] Institute of Astronomy, University of Hawaii at Manoa, USA
[4] Mullard Space Science Laboratory, University College London, UK
[5] IRAP, Universite de Toulouse, CNRS, CNES, UPS, 31028 Toulouse, France

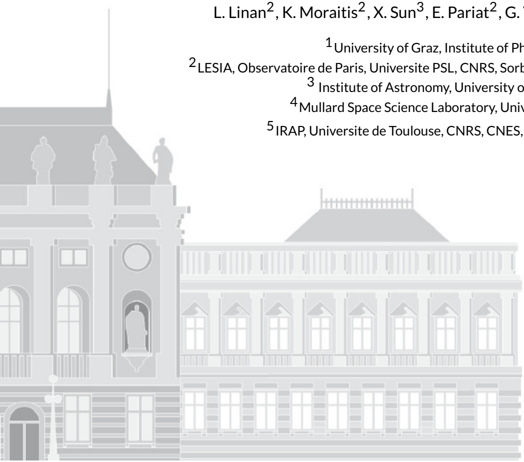

HELICITY 2020
Program on Helicities in Astrophysics

FWF
Der Wissenschaftsfonds.

INTERNATIONAL SPACE SCIENCE INSTITUTE

SOLAR ACTIVE-REGION MAGNETIC FIELD – Observation & Measurement

- ARs at coronal temperatures appear as clusters of loops

  $\longrightarrow$ anchored in regions of opposite magnetic polarity at the photosphere
- 3D magnetic field vector is NOT routinely measured

  (weak fields, high temperatures $\longrightarrow$ weak Zeeman splitting, e.g., *Cargill, 2009)*
- Lack of measurements is compensated by:

  "EXTRAPOLATION" of the surface field into the corona

  $\longrightarrow$ Approximate $\boldsymbol{B}$ in the 3D corona based on measured photospheric $\boldsymbol{B}$

  $\longrightarrow$ Once coronal $\boldsymbol{B}$ is known physical conditions can be studied

- ARs in near-surface layers are characterized by a bipolar pattern

  $\longrightarrow$ clusters of opposite magnetic polarity
- 3D photospheric magnetic field vector is routinely measured

  (strong field, low temperatures $\longrightarrow$ pronounced Zeeman effect)

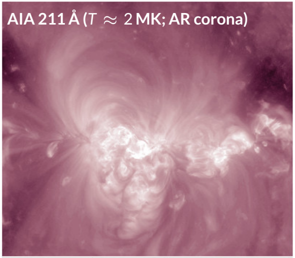

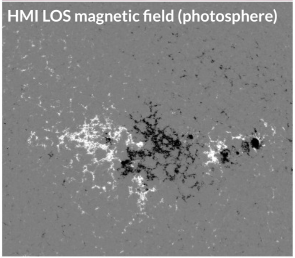

Credit: NASA/ESA/JAXA

SOLAR ACTIVE-REGION MAGNETIC FIELD – Importance of modeling

- Intrinsic to the emergence of magnetic field that interacts with the overlying field active region field: FLARES and ERUPTIONS
- Energy that fuels solar eruptions can, by comparison, only stem from that previously stored in the continuously evolving (coronal) magnetic field

  But energy is dissipative! $\longrightarrow$ Need for a quantity uniquely related to topological changes
- MAGNETIC HELICITY is (almost) conserved in (resistive) ideal MHD

  (Woltjer, 1958; Taylor, 1974; Pariat et al.*, 2015)*

  Explanation for existence of plasma ejecta

  $\longrightarrow$ to prevent infinite accumulation within the solar corona *(Rust, 1994; Low, 1996)*

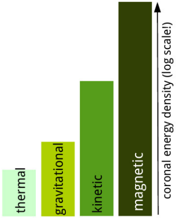

Coronal energy reservoir. Shown are the contributions of thermal, gravitational, kinetic and magnetic energy density in logarithmic scale (Forbes, 2000).

SOLAR ACTIVE-REGION MAGNETIC FIELD – Force-free approximation

The equations to be solved are:

$$
\begin{aligned}
\nabla \cdot \boldsymbol{B} &= 0, && (1)\\
\nabla \times \boldsymbol{B} &= \mu_0 \boldsymbol{J}, && (2)\\
\boldsymbol{J} \times \boldsymbol{B} = (\nabla \times \boldsymbol{B}) \times \boldsymbol{B} &= 0. && (3)
\end{aligned}
$$

A vanishing Lorentz force (3) can be fulfilled

by $\nabla \times \boldsymbol{B} = 0$ $(\rightarrow \boldsymbol{J} = 0$, *current-free*, *potential*),

or $\nabla \times \boldsymbol{B} \parallel \boldsymbol{B}$ (force-free).

The force-free equation, in combination with (2), can be rewritten as

$$\mu_0 \boldsymbol{J} = \alpha_{\mathrm{ff}} \boldsymbol{B} \qquad (\boldsymbol{J} \text{ and } \boldsymbol{B} \text{ aligned and proportional}), \qquad (4)$$

Taking the divergence of (4) yields

$$\boldsymbol{B} \cdot \nabla \alpha_{\mathrm{ff}} = 0 \qquad (\alpha_{\mathrm{ff}} \text{ constant along a given field line, but may vary along individual field lines}). \qquad (5)$$

If $\alpha_{\mathrm{ff}} = f(\boldsymbol{r}) \rightarrow$ NONLINEAR FORCE-FREE (NLFF) field.

NLFF MODELING – A non-trivial task

Different methods to solve the set of equations in the NLFF case (1), (2) and (5) exist.
(See reviews by, e.g., *Wiegelmann (2008); Wiegelmann and Sakurai (2012).*)

Successful application of NLFF methods requires, at a minimum
(Schrijver et al., *2006; Metcalf* et al., *2008; Schrijver* et al., *2008; De Rosa* et al., *2009; DeRosa* et al., *2015)*

- Realism: Good alignment of modeled field lines to observed coronal loops
- Consistency: Acceptable agreement of the α_{ff}-correspondence relation
- Quality: Low values of standard quality metrics *(Schrijver* et al., *2006; Wheatland* et al., *2000)*

and from a computational point of view, in addition:

- Large model volumes of high spatial resolution

  $\rightarrow$ accommodate the essential field line connectivity within a solar active region, as well the connectivity to its surrounding
- Accommodate measurement uncertainties

  $\rightarrow$ in particular that of the transverse magnetic field component *(e.g., Wiegelmann and Inhester, 2010)*
- Acquire force-free consistent model input

  $\rightarrow$ "preprocessing" *(e.g., Wiegelmann* et al., *2006; Fuhrmann* et al., *2007, 2011)*

NLFF MODELING – Optimization method

We use the OPTIMIZATION method *(Wiegelmann, 2004; Wiegelmann and Inhester, 2010)*
to find an approximate solution to the NLFF problem, by minimizing

$$
\begin{aligned}
L &= \int_V w_{\mathrm{f}} \frac{|(\nabla \times \boldsymbol{B}) \times \boldsymbol{B}|^2}{B^2} + w_{\mathrm{d}} |\nabla \cdot \boldsymbol{B}|^2 \, \mathrm{d}V \\
&+ \nu \int_S (\boldsymbol{B} - \boldsymbol{B}_{\mathrm{obs}}) \cdot \boldsymbol{W} \cdot (\boldsymbol{B} - \boldsymbol{B}_{\mathrm{obs}}) \, \mathrm{d}S
\end{aligned}
\tag{6}
$$

- Constrains (2) as quadratic form. (Fulfilled for $w_{\mathrm{f}} > 0$.).
- Constrains (1) as quadratic form. (Fulfilled for $w_{\mathrm{d}} > 0$.).

  Evidently, when L is minimal, the force-free conditions are fulfilled.
- Constrains the model field, $\boldsymbol{B}$, at $z = 0$ using a diagonal error matrix $\boldsymbol{W}(x, y)$.

  $\rightarrow$ Diagonal elements are inversely proportional to the local measurement uncertainty.

After successful minimization of (6), we can study the approximated 3D coronal $\boldsymbol{B}$, thus its MAGNETIC HELICITY.

MAGNETIC HELICITY – Relative magnetic helicity

A gauge-invariant helicity (i.e., applicable for solar cases) can be defined as
(Berger and Field, 1984; Jensen and Chu, 1984; Finn and Antonsen, 1985):

$$H_{\mathcal{V}} \quad = \quad \int_V (\boldsymbol{A} + \boldsymbol{A}_{\rm p}) \cdot (\boldsymbol{B} - \boldsymbol{B}_{\rm p})\, {\rm d}V, \tag{7}$$

with respect to a reference (potential) field, $\boldsymbol{B}_{\rm p}$, with the particular property $B_n = B_{{\rm p},n}$.

Possible decomposition of $H_{\mathcal{V}}$ *(Berger, 2003)*:

$$H_{\mathcal{V}} \quad = \quad H_{\rm J} + 2H_{\rm PJ}, \tag{8}$$

$$H_{\rm J} \quad = \quad \int_V (\boldsymbol{A} - \boldsymbol{A}_{\rm p}) \cdot (\boldsymbol{B} - \boldsymbol{B}_{\rm p})\ {\rm d}V, \tag{9}$$

$\longrightarrow$ (self-) helicity of the current- carrying field $\boldsymbol{B}_c = \boldsymbol{B} - \boldsymbol{B}_{\rm p}$

$$H_{\rm PJ} \quad = \quad \int_V \boldsymbol{A}_{\rm p} \cdot (\boldsymbol{B} - \boldsymbol{B}_{\rm p})\ {\rm d}V. \tag{10}$$

$\longrightarrow$ helicity of the volume-threading field

MAGNETIC HELICITY – Relative magnetic helicity

A gauge-invariant helicity (i.e., applicable for solar cases) can be defined as *(Berger and Field, 1984; Jensen and Chu, 1984; Finn and Antonsen, 1985)*:

$$H_{\mathcal{V}} = \int_V (\boldsymbol{A} + \boldsymbol{A}_{\mathrm{p}}) \cdot (\boldsymbol{B} - \boldsymbol{B}_{\mathrm{p}})\, \mathrm{d}V, \tag{7}$$

with respect to a reference (potential) field, $\boldsymbol{B}_{\mathrm{p}}$, with the particular property $B_n = B_{\mathrm{p},n}$.

Possible decomposition of $H_{\mathcal{V}}$ *(Berger, 2003)*:

$$H_{\mathcal{V}} = H_{\mathrm{J}} + 2H_{\mathrm{PJ}}, \tag{8}$$

$$H_{\mathrm{J}} = \int_V (\boldsymbol{A} - \boldsymbol{A}_{\mathrm{p}}) \cdot (\boldsymbol{B} - \boldsymbol{B}_{\mathrm{p}})\, \mathrm{d}V, \tag{9}$$

$$H_{\mathrm{PJ}} = \int_V \boldsymbol{A}_{\mathrm{p}} \cdot (\boldsymbol{B} - \boldsymbol{B}_{\mathrm{p}})\, \mathrm{d}V. \tag{10}$$

The helicity ratio, $|H_{\mathrm{J}}|/|H_{\mathcal{V}}|$, is indicative for eruptivity!

→ in simulations *(Pariat et al., 2017)*

→ in NLFF model applications to solar observations *(James et al., 2018; Moraitis et al., 2019; Thalmann et al., 2019a)*.

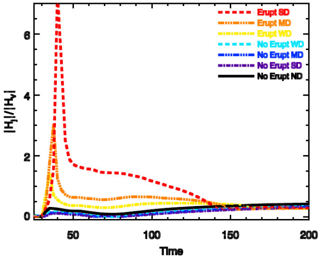

Time evolution of the helicity ratio $|H_{\mathrm{J}}|/|H_{\mathcal{V}}|$ for seven parametric MHD simulations, either eruptive (warm colors) or non-eruptive in nature (cold colors). Adapted from Fig. 7 of Pariat et al. (2017).

FV HELICITY COMPUTATION – A non-trivial task

To determine the 3D magnetic vector potential $\boldsymbol{A}$ one has to solve (for a given solenoidal vector magnetic field):

$$\nabla \times \boldsymbol{B} = \cancel{\nabla(\nabla \cdot \boldsymbol{A})} - \Delta \boldsymbol{A} = \mu_0 \boldsymbol{J}, \tag{11}$$

subject to the boundary requirement

$$\boldsymbol{n} \cdot \boldsymbol{B} = \boldsymbol{n} \cdot (\nabla \times \boldsymbol{A}) \qquad \text{on } \partial \mathrm{V}, \tag{12}$$

and the additional constraint (Coulomb gauge)

$$\nabla \cdot \boldsymbol{A} = 0^{\star)}. \tag{13}$$

$^{\star)}$ *Alternatively, e.g., $A_z = 0$ ("DeVore gauge"; DeVore, 2000) can be used (for a corresponding derivation of $\boldsymbol{A}$ see Valori* et al.*, 2012).*

FV HELICITY COMPUTATION – A non-trivial task

Decomposing $\boldsymbol{B} = \boldsymbol{B}_c + \boldsymbol{B}_\mathrm{p}$, the reference field is defined as $\boldsymbol{B}_\mathrm{p} = \nabla\phi$, where

$$\begin{aligned} \Delta\phi &= 0, && (16) \\ (\boldsymbol{n}\cdot\nabla\phi)\,|_{\partial V} &= (\boldsymbol{n}\cdot\boldsymbol{B})\,|_{\partial V}, && (17) \end{aligned}$$

such that $B_{\mathrm{p},n} = B_n$ is satisfied.

Using the Coulomb gauge *(e.g., Thalmann* et al.*, 2011)* one then has to solve:

$$\begin{aligned} \Delta\boldsymbol{A}_\mathrm{p} &= 0, && (18) \\ \nabla\cdot\boldsymbol{A}_\mathrm{p} &= 0, && (19) \\ \boldsymbol{n}\cdot(\nabla\times\boldsymbol{A}_\mathrm{p})\,|_{\partial V} &= (\boldsymbol{n}\cdot\boldsymbol{B})\,|_{\partial V}. && (20) \end{aligned}$$

$\rightarrow$ $\boldsymbol{A}_\mathrm{p}$ is designed to reproduce the magnetic flux on ∂V.

$$\begin{aligned} \Delta\boldsymbol{A}_c &= -\mu_0\boldsymbol{J}, && (21) \\ \nabla\cdot\boldsymbol{A}_c &= 0, && (22) \\ (\boldsymbol{n}\times\boldsymbol{A}_c)\,|_{\partial V} &= 0. && (23) \end{aligned}$$

$\rightarrow$ $\boldsymbol{A}_c$ reproduces the electric currents.

Then, $\nabla\times\boldsymbol{A} = \nabla\times(\boldsymbol{A}_\mathrm{p}+\boldsymbol{A}_c) = \boldsymbol{B}$ and $H_\mathcal{V}$ in (7) is gauge-invariant.

FV HELICITY COMPUTATION – A non-trivial task

"Finite-volume" (FV) methods to solve the set of equations (18) – (23) exist.
(See review by, e.g., *Valori* et al. *(2016)*.)

Successful application of FV helicity methods requires (at a minimum):

– High degree of solenoidality of the input field $\boldsymbol{B}$
  Reliability lost when energy error exceeds $\sim$10% *(for solar-like MHD test case; Valori* et al., *2016)*.

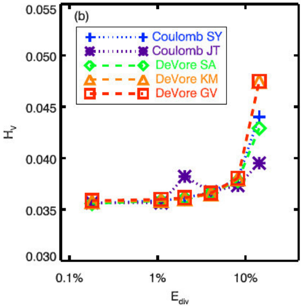

Relative helicity as a function of error on energy from numerical precision (E_{div}). Adapted from Fig. 8 of Valori et al. *(2016).*

FV HELICITY COMPUTATION – A non-trivial task

"Finite-volume" (FV) methods to solve the set of equations (18) – (23) exist.
(See review by, e.g., *Valori* et al. *(2016)*.)

Successful application of FV helicity methods requires (at a minimum):

- High degree of solenoidality of the input field $\boldsymbol{B}$
  Errors might be ignorable as long as energy error is below $\sim$5% *(for solar cases; Thalmann* et al., *2019b)*.

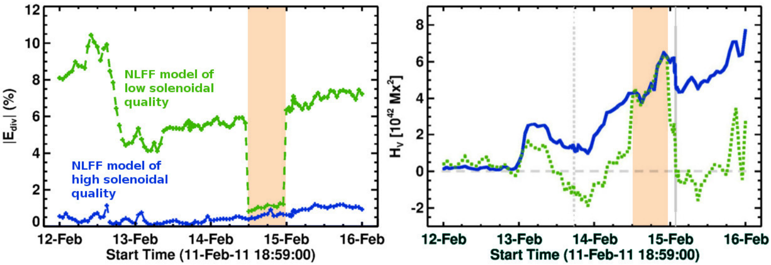

Left: Nonsolenoidal contributions to the magnetic energy, computed following Valori et al. *(2013), in NLFF solutions of lower (green) and high (blue) solenoidal quality. Right: Corresponding total helicity, $H_{\mathcal{V}}$, derived using the FVCoulomb method of Thalmann* et al. *(2011). Vertical dashed and solid lines mark the GOES peak time of M- and X-class flares, respectively. Adapted from Figs. 2 and 3 of Thalmann* et al. *(2019b).*

FV HELICITY COMPUTATION – A non-trivial task

"Finite-volume" (FV) methods to solve the set of equations (18) – (23) exist.
(See review by, e.g., *Valori* et al. *(2016)*.)

Successful application of FV helicity methods requires (at a minimum):

- High degree of solenoidality of the input field $\boldsymbol{B}$
  Errors might be ignorable as long as energy error is below $\sim$5% *(for solar cases; Thalmann* et al., *2019b)*.
- Realistic estimate of model-induced uncertainties *(Thalmann* et al., *2020)*

Remember:
We use the OPTIMIZATION method *(Wiegelmann, 2004; Wiegelmann and Inhester, 2010)* to find an approximate solution to the NLFF problem, by minimizing

$$L = \int_V w_f \frac{|(\nabla \times \boldsymbol{B}) \times \boldsymbol{B}|^2}{B^2} + w_d |\nabla \cdot \boldsymbol{B}|^2 \, dV + \nu \int_S (\boldsymbol{B} - \boldsymbol{B}_{obs}) \cdot \boldsymbol{W} \cdot (\boldsymbol{B} - \boldsymbol{B}_{obs}) \, dS \quad (6)$$

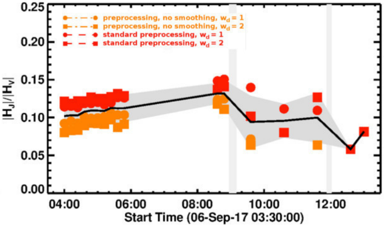

Helicity ratio, $|H_J|/|H_\mathcal{V}|$*, as a function of time around two major X-class flares in AR 12673. The black solid line represents the mean value, the gray-shaded area marks the spread (standard deviation). Vertical bars mark the impulsive phases. Adapted from Fig. 5 of Thalmann* et al. *(2020).*

HELICITY RATIO – Potential for flare prediction

Pilot study of two exemplary ARs *(Thalmann* et al., *2019a)*:

- larger helicity ratio in CME-productive NOAA 11158 ($|H_J|/|H_{\mathcal{V}}| \gtrsim 0.1$)

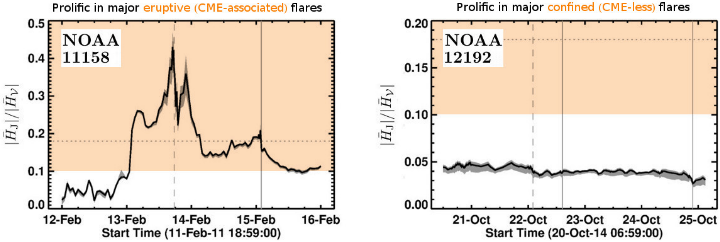

Time evolution of $|H_J|/|H_{\mathcal{V}}|$ during disk passage of NOAA 11158 (CME-productive; left panel) and NOAA 12192 (CME-less; right panel). Vertical dashed/solid lines mark the peak time of M- and X-class flares, respectively. The horizontal dotted line marks a characteristic pre-flare level of $|H_J|/|H_{\mathcal{V}}|$ in CME- productive AR 11158. Adapted from Fig. 3 of Thalmann et al. *(2019a).*

HELICITY RATIO – Potential for flare prediction

Pilot study of two exemplary ARs *(Thalmann* et al.*, 2019a)*:

- larger helicity ratio in CME-productive NOAA 11158 ($|H_J|/|H_\mathcal{V}| \gtrsim 0.1$)
- pronounced flare-related responses

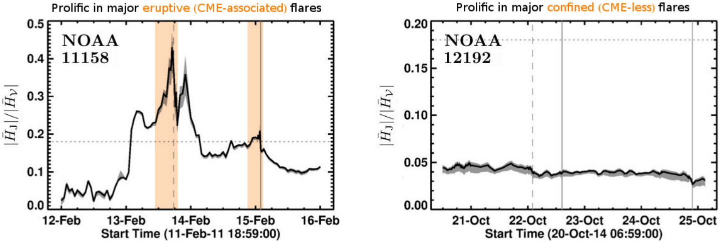

Time evolution of $|H_J|/|H_\mathcal{V}|$ during disk passage of NOAA 11158 (CME-productive; left panel) and NOAA 12192 (CME-less; right panel). Vertical dashed/solid lines mark the peak time of M- and X-class flares, respectively. The horizontal dotted line marks a characteristic pre-flare level of $|H_J|/|H_\mathcal{V}|$ in CME- productive AR 11158. Adapted from Fig. 3 of Thalmann et al. *(2019a).*

HELICITY RATIO – Potential for flare prediction

Follow-up study of 12 solar ARs seems to confirm the previously found trends *(Gupta et al., in preparation)*.

- higher characteristic values in CME-productive ARs ($|H_J|/|H_\mathcal{V}| \gtrsim 0.1$)
- lower characteristic values in CME-less ARs ($|H_J|/|H_\mathcal{V}| \lesssim 0.1$)

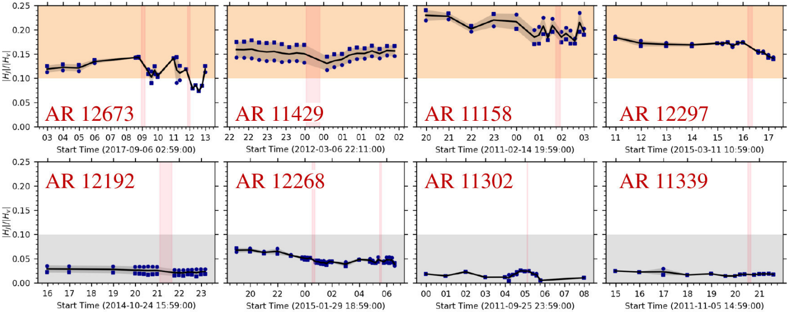

Helicity ratio of CME-productive (top row) and CME-less (bottom row) ARs, around the time of the largest respective flare produced. Vertical bars mark the respective impulsive phases. Orange- and gray-shaded areas mark characteristic pre-flare levels of $|H_J|/|H_\mathcal{V}|$. (Gupta et al., in prep.)

HELICITY RATIO – Open questions

Explanation of atypical CME-productive ARs

$\rightarrow$ $|H_J|/|H_\mathcal{V}| < 0.1$ contrary to expectation

$\rightarrow$ but also $E_F/E_P \lesssim 0.2$

$\rightarrow$ joint interpretation of energy and helicity budgets appears essential

Helicity ratio (top) and energy ratio (bottom) of two exemplary CME-productive ARs, around the time of the largest respective flare produced. Vertical bars mark the respective impulsive phases. Orange- and gray-shaded areas mark characteristic pre-flare levels of $|H_J|/|H_\mathcal{V}|$. (Gupta et al., in prep.)

HELICITY RATIO – Open questions

Need to understand the response to coronal dynamics *(Green et al., in preparation)*

$\rightarrow$ flux emergence vs. small-scale dynamics vs. flare processes

$\rightarrow$ only if understood helicity-based flare prediction may be facilitated

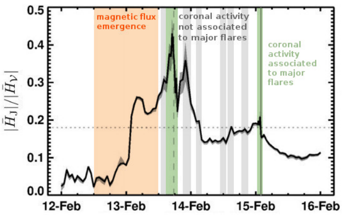

Time evolution of $|H_J|/|H_\mathcal{V}|$ *(left) and* E_F/E_P *(right) during disk passage of NOAA 11158. Vertical lines mark major M- and X-class flares. Gray bars mark times of activity not associated to M- or X-class flares. The horizontal dotted line marks a characteristic pre-flare level of* $|H_J|/|H_\mathcal{V}|$ *in CME- productive ARs. Adapted from Fig. 3 of Thalmann* et al. *(2019a) and Fig. 4a of Sun* et al. *(2012).*

SUMMARY

Understanding of coronal (eruptive) processes requires:

→ investigation of non-dissipative quantities such as (relative) magnetic helicity
(unique relation to changes of the magnetic field geometry)

→ in relation with dissipative ones as, e.g., magnetic energy
(seems to be more sensitive to, e.g., flare size)

Success in modeling of coronal processes requires (among others):

→ high-quality modeling of the 3D (NLFF) coronal magnetic field
(in terms of force- and divergence freeness, as well as its realism)

→ reliable computation of the coronal relative helicity

Monitoring the relative helicity and energy for a large number of ARs and based longer time series (with high temporal cadence) will allow it to:

→ better understand responses to coronal dynamics on different spatial scales

→ possibly aid flare forecasting schemes

References I

Berger, M. A. (2003). *Topological quantities in magnetohydrodynamics*, pages 345–374.

Berger, M. A. and Field, G. B. (1984). The topological properties of magnetic helicity. *J. Fluid Mech.*, **147**, 133–148.

Cargill, P. J. (2009). Coronal Magnetism: Difficulties and Prospects. *Space Sci. Rev.*, **144**(1-4), 413–421.

De Rosa, M. L., Schrijver, C. J., Barnes, G., Leka, K. D., Lites, B. W., Aschwanden, M. J., Amari, T., Canou, A., McTiernan, J. M., Régnier, S., Thalmann, J. K., Valori, G., Wheatland, M. S., Wiegelmann, T., Cheung, M. C. M., Conlon, P. A., Fuhrmann, M., Inhester, B., and Tadesse, T. (2009). A Critical Assessment of Nonlinear Force-Free Field Modeling of the Solar Corona for Active Region 10953. *Astrophys. J.*, **696**(2), 1780–1791.

DeRosa, M. L., Wheatland, M. S., Leka, K. D., Barnes, G., Amari, T., Canou, A., Gilchrist, S. A., Thalmann, J. K., Valori, G., Wiegelmann, T., Schrijver, C. J., Malanushenko, A., Sun, X., and Régnier, S. (2015). The Influence of Spatial resolution on Nonlinear Force-free Modeling. *Astrophys. J.*, **811**(2), 107.

DeVore, C. R. (2000). Magnetic Helicity Generation by Solar Differential Rotation. *Astrophys. J.*, **539**(2), 944–953.

Finn, J. M. and Antonsen, J. T. M. (1985). Magnetic helicity: what is it and what is it good for. *Comments Plasma Phys. Controlled Fusion; (United Kingdom)*, **9:3**.

Forbes, T. (2000). *Solar Flare Models*, page 2295.

Fuhrmann, M., Seehafer, N., and Valori, G. (2007). Preprocessing of solar vector magnetograms for force-free magnetic field extrapolation. *Astron. Astrophys.*, **476**(1), 349–357.

Fuhrmann, M., Seehafer, N., Valori, G., and Wiegelmann, T. (2011). A comparison of preprocessing methods for solar force-free magnetic field extrapolation. *Astron. Astrophys.*, **526**, A70.

James, A. W., Valori, G., Green, L. M., Liu, Y., Cheung, M. C. M., Guo, Y., and van Driel-Gesztelyi, L. (2018). An Observationally Constrained Model of a Flux Rope that Formed in the Solar Corona. *Astrophys. J.*, **855**, L16.

Jensen, T. H. and Chu, M. S. (1984). Current drive and helicity injection. *Physics of Fluids*, **27**(12), 2881–2885.

Low, B. C. (1996). Solar Activity and the Corona. *Sol. Phys.*, **167**(1-2), 217–265.

Metcalf, T. R., De Rosa, M. L., Schrijver, C. J., Barnes, G., van Ballegooijen, A. A., Wiegelmann, T., Wheatland, M. S., Valori, G., and McTtiernan, J. M. (2008). Nonlinear Force-Free Modeling of Coronal Magnetic Fields. II. Modeling a Filament Arcade and Simulated Chromospheric and Photospheric Vector Fields. *Sol. Phys.*, **247**(2), 269–299.

Moraitis, K., Sun, X., Pariat, É., and Linan, L. (2019). Magnetic helicity and eruptivity in active region 12673. *Astron. Astrophys.*, **628**, A50.

Pariat, E., Valori, G., Démoulin, P., and Dalmasse, K. (2015). Testing magnetic helicity conservation in a solar-like active event. *Astron. Astrophys.*, **580**, A128.

Pariat, E., Leake, J. E., Valori, G., Linton, M. G., Zuccarello, F. P., and Dalmasse, K. (2017). Relative magnetic helicity as a diagnostic of solar eruptivity. *Astron. Astrophys.*, **601**, A125.

Rust, D. M. (1994). Spawning and Shedding Helical Magnetic Fields in the Solar Atmosphere. *Geophys. Res. Lett.*, **21**(4), 241–244.

Schrijver, C. J., De Rosa, M. L., Metcalf, T. R., Liu, Y., McTiernan, J., Régnier, S., Valori, G., Wheatland, M. S., and Wiegelmann, T. (2006). Nonlinear Force-Free Modeling of Coronal Magnetic Fields Part I: A Quantitative Comparison of Methods. *Sol. Phys.*, **235**(1-2), 161–190.

Schrijver, C. J., DeRosa, M. L., Metcalf, T., Barnes, G., Lites, B., Tarbell, T., McTiernan, J., Valori, G., Wiegelmann, T., Wheatland, M. S., Amari, T., Aulanier, G., Démoulin, P., Fuhrmann, M., Kusano, K., Régnier, S., and Thalmann, J. K. (2008). Nonlinear Force-free Field Modeling of a Solar Active Region around the Time of a Major Flare and Coronal Mass Ejection. *Astrophys. J.*, **675**(2), 1637–1644.

References II

Sun, X., Hoeksema, J. T., Liu, Y., Wiegelmann, T., Hayashi, K., Chen, Q., and Thalmann, J. (2012). Evolution of Magnetic Field and Energy in a Major Eruptive Active Region Based on SDO/HMI Observation. *Astrophys. J.*, **748**(2), 77.

Taylor, J. B. (1974). Relaxation of Toroidal Plasma and Generation of Reverse Magnetic Fields. *Phys. Rev. Lett.*, **33**(19), 1139–1141.

Thalmann, J. K., Inhester, B., and Wiegelmann, T. (2011). Estimating the Relative Helicity of Coronal Magnetic Fields. *Sol. Phys.*, **272**(2), 243–255.

Thalmann, J. K., Moraitis, K., Linan, L., Pariat, E., Valori, G., and Dalmasse, K. (2019a). Magnetic Helicity Budget of Solar Active Regions Prolific of Eruptive and Confined Flares. *Astrophys. J.*, **887**(1), 64.

Thalmann, J. K., Linan, L., Pariat, E., and Valori, G. (2019b). On the Reliability of Magnetic Energy and Helicity Computations Based on Nonlinear Force-free Coronal Magnetic Field Models. *Astrophys. J. Lett.*, **880**(1), L6.

Thalmann, J. K., Sun, X., Moraitis, K., and Gupta, M. (2020). On the Reliability of Relative Helicities Deduced From Nonlinear Force-free Coronal Models. *Astron. Astrophys.*, **accepted**.

Valori, G., Démoulin, P., and Pariat, E. (2012). Comparing Values of the Relative Magnetic Helicity in Finite Volumes. *Sol. Phys.*, **278**(2), 347–366.

Valori, G., Démoulin, P., Pariat, E., and Masson, S. (2013). Accuracy of magnetic energy computations. *Astron. Astrophys.*, **553**, A38.

Valori, G., Pariat, E., Anfinogentov, S., Chen, F., Georgoulis, M. K., Guo, Y., Liu, Y., Moraitis, K., Thalmann, J. K., and Yang, S. (2016). Magnetic Helicity Estimations in Models and Observations of the Solar Magnetic Field. Part I: Finite Volume Methods. *Space Sci. Rev.*, **201**(1-4), 147–200.

Wheatland, M. S., Sturrock, P. A., and Roumeliotis, G. (2000). An Optimization Approach to Reconstructing Force-free Fields. *Astrophys. J.*, **540**(2), 1150–1155.

Wiegelmann, T. (2004). Optimization code with weighting function for the reconstruction of coronal magnetic fields. *Sol. Phys.*, **219**(1), 87–108.

Wiegelmann, T. (2008). Nonlinear force-free modeling of the solar coronal magnetic field. *J. Geophys. Res.(Space Physics)*, **113**(A3), A03S02.

Wiegelmann, T. and Inhester, B. (2010). How to deal with measurement errors and lacking data in nonlinear force-free coronal magnetic field modelling? *Astron. Astrophys.*, **516**, A107.

Wiegelmann, T. and Sakurai, T. (2012). Solar Force-free Magnetic Fields. *Living Rev. Sol. Phys.*, **9**(1), 5.

Wiegelmann, T., Inhester, B., and Sakurai, T. (2006). Preprocessing of Vector Magnetograph Data for a Nonlinear Force-Free Magnetic Field Reconstruction. *Sol. Phys.*, **233**(2), 215–232.

Woltjer, L. (1958). On Hydromagnetic Equilibrium. *Proceedings of the National Academy of Science*, **44**(9), 833–841.